

Quantum Phase Transitions of Bilayer Spin-orbit Coupled Bose-Einstein Condensates

Qing Sun,¹ Lin Wen,² W.-M. Liu,² G. Juzeliūnas,^{3,*} and An-Chun Ji^{1,†}

¹*Department of Physics, Capital Normal University, Beijing 100048, China*

²*Beijing National Laboratory for Condensed Matter Physics,
Institute of Physics, Chinese Academy of Sciences, Beijing 100190, China*

³*Institute of Theoretical Physics and Astronomy,
Vilnius University, A. Goštauto 12, Vilnius 01108, Lithuania*

(Dated: March 19, 2014)

We investigate the ground state structures of a bilayer atomic Bose-Einstein condensate (BEC). Each layer is subjected to a one-dimensional (1D) spin-orbit coupling (SOC) in a different direction, effectively providing a 2D SOC. The interplay between the interlayer tunneling, SOC and intralayer atomic interaction gives rise to a diverse phase diagram. We demonstrate that the system can undergo a transition to a new type of stripe phase which spontaneously breaks the time-reversal symmetry. Different from the ordinary Rashba-type SOC, a half-skyrmion lattice can emerge spontaneously in the bilayer system without strong harmonic traps. Furthermore, we predict the occurrence of a tetracritical point in the phase diagram of the bilayer BEC, where four different quantum phases merge together. The origin of the emerging different phases is elucidated.

PACS numbers: 67.85.-d, 03.75.Mn, 05.30.Jp

The search for new exotic quantum states [1, 2] and the study of quantum phase transitions (QPTs) [3] are currently amongst the main issues in the condensed matter community. During the last few years these topics have gained an increasing interest for ultracold atomic gases [4–8] which represent the systems simulating many condensed matter phenomena. Recent experimental progress in the spin-orbit coupling (SOC) of degenerate atomic gases [9–13] has stimulated the theoretical studies of diverse new quantum phases due to the SOC [8, 14, 15], such as emergence of the stripe phase in atomic Bose-Einstein condensates (BECs) [16–20], or formation of unconventional bound states [21–24] and topological superfluidity [25] for atomic fermions. It was demonstrated that for the spin-orbit (SO) coupled BECs, the half-vortex (meron) ground states may develop in strong harmonic traps [26–29]. Such topological objects are of special interest for studying the nontrivial spin configurations in condensed matter physics [30–33].

Although most of the exotic phases have been investigated for the two-dimensional (2D) Rashba-type SOC, its experimental realization remains a challenge for ultracold atoms [8, 34–42]. So far, only a special case of an equal weight of Rashba and Dresselhaus SOC representing the 1D SOC of the form $\propto k_x \sigma_x$ (or $\propto k_y \sigma_x$), has been realized experimentally [9–13].

In this Letter we show that an effective 2D SOC can be produced by means of a more accessible bilayer atomic system. The atoms in each layer are affected by the 1D SOC in a different direction, along the \hat{x} and \hat{y} axis respectively. The bilayer introduces an extra degree of freedom playing an important role in many exotic quantum phenomena [43–46]. Here, the effective 2D SOC is induced via the interlayer tunneling which mixes the chiral states of individual layers subjected to the 1D SOC.

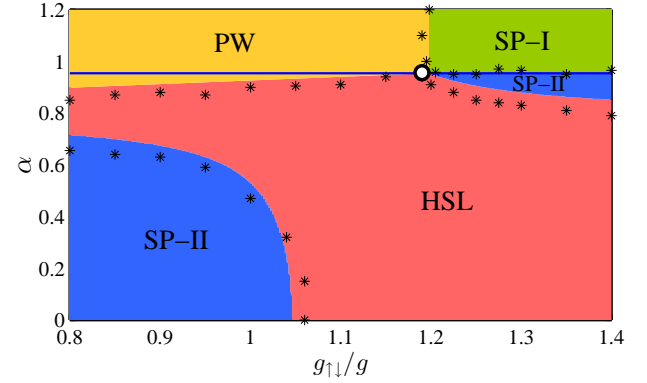


FIG. 1: (color online) Phase diagram of a bilayer BEC with an effective 2D SOC as a function of the dimensionless interlayer tunneling α and relative atomic interaction $g_{\uparrow\downarrow}/g$. Here, the dimensionless intralayer coupling is set to be $\beta = 0.3$. The stars represent the phase boundaries determined from the numerical simulations. A tetracritical point (TP) marked by a circle occurs on the critical line $\alpha^2 + \beta^2 = 1$ (the horizontal solid line). The colored regions are determined by variational calculations, denoting normal stripe (SP-I, green) and plane-wave (PW, yellow) phases, a new type of stripe phase (SP-II, blue), as well as a half skyrmion lattice (HSL, red) phase.

Compared to the ordinary Rashba-type SOC, the extra bilayer degree of freedom gives rise to additional intriguing ground state structures controlled by the intralayer atomic interactions. This provides a new way for exploring diverse exotic quantum states and novel QPTs.

Our main findings are summarized in Fig. 1. For a large interlayer tunneling the two layers are strongly coupled, leading to the normal stripe (SP-I) and plane-wave (PW) phases. For a moderate tunneling, the system develops a new type of stripe phase (SP-II), which chooses spontaneously a pair of asymmetric wave vectors

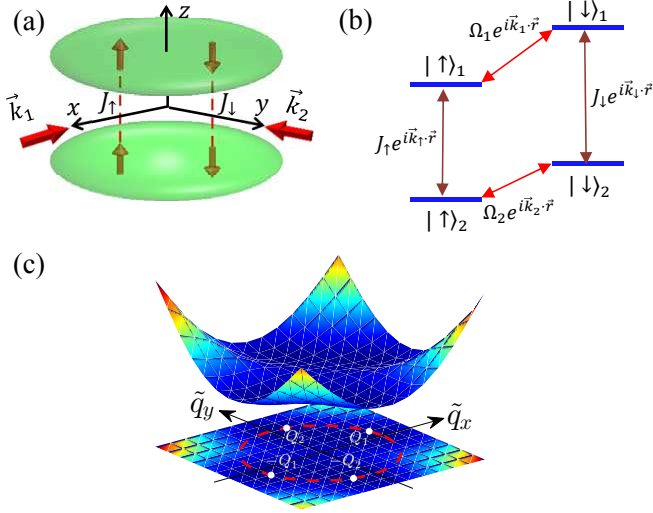


FIG. 2: (color online) (a) Schematic diagram of the bilayer system where the atoms are characterized by two internal states $\sigma = \uparrow, \downarrow$. For each layer the laser beams induce transitions between the atomic internal states with the coupling strength $\Omega_{1,2}$ and the recoil momenta $\mathbf{k}_{1,2}$ along the \hat{x} and \hat{y} axis respectively; J_σ is the effective strength of the laser induced interlayer tunnelling for each internal state σ . (b) Setup for laser coupled intralayer states and laser-assisted interlayer tunnelling of the bilayer atoms. (c) Band structure of the single particle Hamiltonian \hat{H}_{eff} , Eq. (S12), for the relative interlayer tunnelling $\alpha = 0.6$ and intralayer coupling $\beta = 0.3$. There are four degenerate minima at $\pm \mathbf{Q}_1$ and $\pm \mathbf{Q}_2$ in the lowest band.

and breaks the time-reversal (TR) symmetry. Significantly, a half-skyrmion lattice (HSL) phase emerges now in a wide range of parameters and forms a *spontaneous ground state* in *homogeneous* BECs. This is in contrast to other skyrmions induced by strong traps [26, 28, 29] or thermal quenching [47] in Rashba-type SO coupled BECs, as well as by phase-imprinting [48, 49]. Moreover, we show that a tetracritical point (TP) occurs among the four different quantum phases. This fundamental aspect of phase transitions [50] was first found in anisotropic antiferromagnets [51, 52] and has never been predicted for ultracold atoms.

The system under investigation is depicted in Fig. 2(a), where an atomic BEC is confined in a bilayer geometry. The atoms are characterized by two internal (quasi-spin) states labeled by the index $\sigma = \uparrow, \downarrow$. These can be, e.g., two magnetic sub-levels of the $F = 1$ ground state manifold of the ^{87}Rb -type alkali atoms [9], or a spin-singlet ground state and a long-lived spin triplet excited state of alkaline-earth atoms [1].

Within an individual layer $j = 1, 2$ the laser beams induce transitions between the atomic internal states with the coupling strength Ω_j . The associated recoil momentum \mathbf{k}_j is along the \hat{x} or \hat{y} axis depending on the layer $j = 1, 2$. On the other hand, the direct interlayer tunnel-

ing is inhibited due to a large asymmetry in the double-well potential. In that case one can rely exclusively on the laser-assisted interlayer tunnelling [2–5] characterized by the effective strength J_σ and intralayer momentum transfer \mathbf{k}_σ , as shown in Fig. 2(b). The interlayer coupling $J_\sigma = \Omega_\sigma \int dz \phi_{2\sigma}^*(z) \phi_{1\sigma}(z) e^{ik_z z}$ is determined by both the Rabi frequency Ω_σ of the atom-light coupling and also the overlap integral of the mode functions $\phi_{j\sigma}(z)$ for different layers. It is noteworthy that the laser-induced interlayer tunnelling can take place only if there is a momentum transfer k_z in the tunnelling direction z [4]. In fact, the eigen-states corresponding to each layer $\phi_{1\sigma}(z)$ and $\phi_{2\sigma}(z)$ are orthogonal, so it is the factor $e^{ik_z z}$ which makes the overlap integral J_σ non-zero.

We shall consider a symmetric situation where $\Omega_j = \Omega$ and $J_\sigma = J$. By setting $\mathbf{k}_{\uparrow,\downarrow} = \pm(\mathbf{k}_2 - \mathbf{k}_1)/2$ and performing a unitary transformation to eliminate the temporal and spatial dependence in the original Hamiltonian, one arrives at an effective single-particle Hamiltonian, as presented in detail in the Supplementary material [58]:

$$\hat{H}_{\text{eff}} = \int d^2\mathbf{r} \sum_{j=1,2} \hat{\psi}_j^\dagger(\mathbf{r}) \left[\frac{\mathbf{q}^2}{2} + \lambda_j q_j \sigma_x + \Omega \sigma_z \right] \hat{\psi}_j(\mathbf{r}) + J \int d^2\mathbf{r} \sum_{\sigma=\uparrow,\downarrow} \left(\hat{\psi}_{1\sigma}^\dagger(\mathbf{r}) \hat{\psi}_{2\sigma}(\mathbf{r}) + \text{H.c.} \right), \quad (1)$$

where the SOC in each layer is along \hat{x} and \hat{y} directions, with $q_1 = q_x$ and $q_2 = q_y$ respectively; and $\lambda_j = |\mathbf{k}_j|/2$ is the strength of SOC. We shall consider a symmetric case where $\lambda_j = \lambda$, and define the dimensionless wave vector $\tilde{\mathbf{q}} \equiv \mathbf{q}/\lambda$, interlayer tunnelling $\alpha \equiv J/E_\lambda$, and intralayer coupling $\beta \equiv \Omega/E_\lambda$, with $E_\lambda = \lambda^2/2$.

We start with a single-particle spectrum for the Hamiltonian (S12) analyzed in detail in the Sec. B of the Supplementary material [58]. For $\alpha = 0$, the two layers are decoupled, and we have two pairs of degenerate energy minima along the \tilde{q}_x and \tilde{q}_y directions, respectively. By increasing α , the interlayer tunneling couples the two pairs of minima together, resulting in the four minimum chiral states at $\pm \mathbf{Q}_1 = \pm(\tilde{q}_0^+, \tilde{q}_0^-)$ and $\pm \mathbf{Q}_2 = \pm(\tilde{q}_0^-, \tilde{q}_0^+)$, where $\tilde{q}_0^\pm = \frac{1}{2}(\sqrt{Q_0^2 + \alpha^2/2} \pm \sqrt{Q_0^2 - \alpha^2/2})$, with $Q_0 = |\mathbf{Q}_{1,2}|$ satisfying a nonlinear equation [58]. The energy minima contain a reflection symmetry upon the diagonal axis, as shown in Fig. 2(c). When α is increased above the critical line with $\alpha^2 + \beta^2 = 1$, the energy minima of the chiral states converge to $\pm \mathbf{Q}$, with $\mathbf{Q} = \sqrt{1 - \beta^2}(1/2, 1/2)$ situated on the diagonal axis. In this case, for strong intralayer coupling $\beta \geq 1$, the minima would shrink to $\mathbf{Q} = \mathbf{0}$.

For the bilayer quasi-spin 1/2 BEC, the general form of atomic interactions can be written as

$$\hat{H}_{\text{int}} = \int d^2\mathbf{r} \sum_{j=1,2} \left(\frac{g_\uparrow}{2} \hat{n}_{j\uparrow}^2 + \frac{g_\downarrow}{2} \hat{n}_{j\downarrow}^2 + g_{\uparrow\downarrow} \hat{n}_{j\uparrow} \hat{n}_{j\downarrow} \right), \quad (2)$$

where $g_{\uparrow,\downarrow}$ and $g_{\uparrow\downarrow}$ are the intra- and inter-species atomic interactions with $\hat{n}_{j\sigma} = \hat{\psi}_{j\sigma}^\dagger \hat{\psi}_{j\sigma}$. We shall first consider

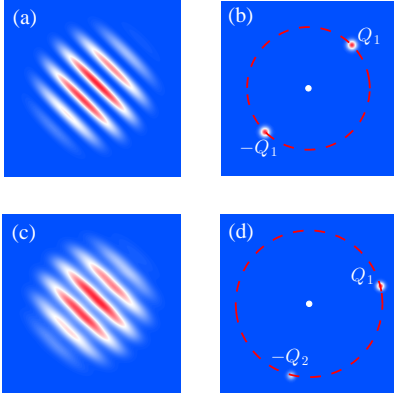


FIG. 3: (Color online) Numerical density profiles of $|\psi_{1\uparrow}(\mathbf{r})|$ and corresponding momentum distributions of $|\psi_{1\uparrow}(\tilde{\mathbf{q}})|$ for the (a,b) normal SP-I ($\alpha = 1.1, g_{\uparrow\downarrow}/g = 1.3$) and (c,d) SP-II ($\alpha = 0.5, g_{\uparrow\downarrow}/g = 0.9$) phases.

the symmetric intra-species interaction with $g_{\uparrow,\downarrow} = g$. The ground state structures can then be investigated by numerically solving the Gross-Pitaevskii (G-P) equations. To this end, we introduce the condensate order parameter $\psi_{j\sigma} \equiv \langle \hat{\psi}_{j\sigma} \rangle$, and include a sufficiently weak harmonic trap with a frequency far less than the SOC frequency E_λ . Then, by minimizing the energy functional $\mathcal{E}[\psi_{j\sigma}] = \langle \hat{H}_{\text{eff}} + \hat{H}_{\text{int}} \rangle$ via the imaginary time evolution method, we derive various quantum phases as shown by the stars in Fig. 1.

To reveal the underlying physics of the phases, we explore whether it is possible for the bilayer atoms to condense with two pairs of wave vectors $\pm\mathbf{Q}_1$ and $\pm\mathbf{Q}_2$ simultaneously. For a spin-1/2 BEC with the Rashba-type SOC, it is quite rare to find a ground state which involves an interference of more than one pair of wave vectors [16]. Even if a square lattice is added to break the translational symmetry leading to the four minimum chiral states, the G-P ground states still favor the normal stripe phase [59]. Only strong traps can mix all lowest energy states with a ring degeneracy, forming a meron ground state with a nonzero angular momentum [26–29]. In a 2D Rashba-type system without strong traps, a state with more than one pair of wave vectors has a non-uniform density modulation and is energetically unfavorable.

However, in the proposed bilayer system where only the atoms situated in the same layer interact repulsively, it is more energetically favorable to delocalize the atoms in both layers. In this case, the competition of the intralayer atomic interactions and interlayer tunneling may couple the four minimum energy states in a different manner and lead to various new quantum phases.

To study the possible multi-wave interfering ground states, we take the following Ansatz $\Psi_G = a_{1+}\Psi_{+\mathbf{Q}_1} + a_{1-}\Psi_{-\mathbf{Q}_1} + a_{2+}\Psi_{+\mathbf{Q}_2} + a_{2-}\Psi_{-\mathbf{Q}_2}$, where $\Psi_{\pm\mathbf{Q}_{1,2}} \equiv \Phi_{\pm\mathbf{Q}_{1,2}} e^{\pm i\mathbf{Q}_{1,2}\cdot\mathbf{r}}$ denote four eigen-functions with the minimum energy [58], and $a_{1\pm}, a_{2\pm}$ are complex amplitudes

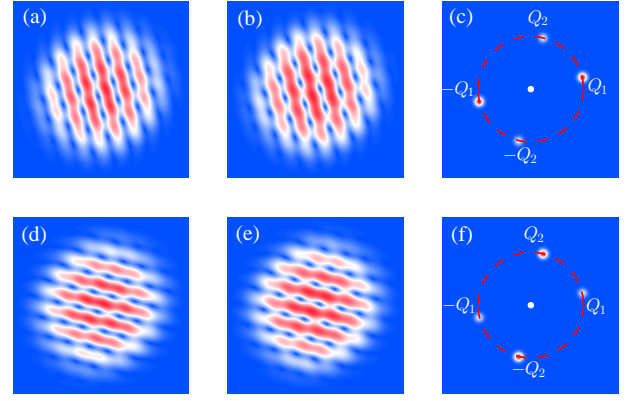


FIG. 4: (Color online) Numerical density profiles of (a,d) $|\psi_{j\uparrow}(\mathbf{r})|$ and (b,e) $|\psi_{j\downarrow}(\mathbf{r})|$ for the HSL phase in each layer ($\alpha = 0.8, g_{\uparrow\downarrow}/g = 1.05$). (c,f) The momentum distributions of $|\psi_{1\sigma}(\tilde{\mathbf{q}})|$ ($|\psi_{2\sigma}(\tilde{\mathbf{q}})|$) for the first (second) layer.

satisfying the normalization condition. By minimizing the energy $\langle \Psi_G | (\hat{H}_{\text{eff}} + \hat{H}_{\text{int}}) | \Psi_G \rangle$, we find that all the emerging phases predicted by the numerical simulations of G-P equations can be identified by the variational results as shown by the colored regions in Fig. 1. This provides a deeper insight into the nature of the ground state configurations.

First, for the large tunneling where $\alpha^2 + \beta^2 > 1$, the two layers are strongly coupled, so that the bilayer behaves like a single layer with the 1D SOC along the diagonal axis. In this case the single-particle Hamiltonian (S12) yields a pair of degenerate eigen-states with the minimum energy and wave vectors $\pm\mathbf{Q}$. Across a critical value of $g_{\uparrow\downarrow}/g$, the condensate transits from the normal SP-I characterized by the wave function $\frac{1}{\sqrt{2}}\Phi_{+\mathbf{Q}}e^{i\mathbf{Q}\cdot\mathbf{r}} + \frac{1}{\sqrt{2}}\Phi_{-\mathbf{Q}}e^{-i\mathbf{Q}\cdot\mathbf{r}}$ to the PW with a single wave vector, as shown in Fig. 1.

Next, we discuss the parameter region $\alpha^2 + \beta^2 < 1$, where the interlayer tunneling mixes the states belonging to different layers in a more sophisticated way, so various nontrivial ground state configurations may appear. In Fig. 3, we show the numerical results of the density and momentum profiles of a spin-up condensate in the first layer for a new type of the stripe phase (SP-II). At first sight, it appears that the density profile of SP-II is similar to that of the normal SP-I (see Fig. 3(a)). However, when we turn to the momentum space, the two types of the stripe phases differ dramatically. For SP-I, the momentum distribution of $|\psi_{j\sigma}(\tilde{\mathbf{q}})|$ comprises a pair of opposite wave vectors $\pm\mathbf{Q}$ which conserve the TR symmetry. Surprisingly, we find that although the ground state wave function of SP-II remains a superposition of two wave vectors, the comprising wave vectors are neither $\pm\mathbf{Q}_1$ nor $\pm\mathbf{Q}_2$. Instead, SP-II becomes a superposition of \mathbf{Q}_1 and $-\mathbf{Q}_2$ which *spontaneously* break the TR symmetry. Basically, this can be understood that

the atoms in one layer are predominantly located at \mathbf{Q}_1 nearly in the \hat{x} -direction, whereas the atoms in another layer dominates at $-\mathbf{Q}_2$ along the \hat{y} -direction, leading to the formation of SP-II phase.

Beyond the SP-II, another distinctive feature in Fig. 1 is that a half skyrmion lattice (HSL) emerges in the ground state. In Fig. 4, a vortex lattice structure can be seen in the density profiles of each spin component. Such lattices of both spin components interlace mutually, forming a coreless structure in each layer. Most notably, the momentum distributions display two pairs of TR invariant momenta, as shown in Fig. 4(c,f). The atoms in each layer tend to be mainly located at $\pm\mathbf{Q}_1$ and $\pm\mathbf{Q}_2$ respectively to make the energy favorable, which indicates that the underlying mechanism of the vortex lattices arises from the four-wave interference with a nontrivial phase structure. To further characterize this state, we calculate the topological charge $Q = \int d^2\mathbf{r} \frac{1}{8\pi} \epsilon^{\mu\nu} \mathbf{S}_j \cdot \partial_\mu \mathbf{S}_j \times \partial_\nu \mathbf{S}_j$ [60]. Here the spin vector are given by $\mathbf{S}_j = (2|\psi_{j\uparrow}||\psi_{j\downarrow}| \cos(\theta_{j\uparrow} - \theta_{j\downarrow}), -2|\psi_{j\uparrow}||\psi_{j\downarrow}| \sin(\theta_{j\uparrow} - \theta_{j\downarrow}), |\psi_{j\uparrow}|^2 - |\psi_{j\downarrow}|^2)$, with $\theta_{j\uparrow}$ ($\theta_{j\downarrow}$) denoting a phase of the spin-up (down) component. Fig. 5(a) shows the spin texture of the up layer (the down layer yields the analogous results), where the skyrmion and antiskyrmion with topological charge $Q = \pm 1/2$ interlace with each other. The total topological charge is zero $Q_T = 0$ and TR symmetry is conserved. This confirms the formation of a HSL, an intriguing topological ground state emerging in such a homogeneous system.

Remarkably, when the interlayer tunneling is tuned to $\alpha^2 + \beta^2 = 1$, a TP may occur on the critical line as marked by the circle in Fig. 1. Indeed, as one starts from the SP-I by decreasing α , the system would first transit across the critical line to the SP-II before entering into the HSL phase. On the other hand, the PW phase extends into the region below the critical line and transits to the HSL directly. Therefore, the TP occurs among the four different quantum phases, which can also be clearly demonstrated in the variational phase diagram.

Having studied the $\alpha - g_{\uparrow\downarrow}/g$ phase diagram, we next discuss the effects of the intralayer coupling β which can be varied conveniently in experiments. For this purpose, we take the parameters $\alpha = 0.6$ and $g_{\uparrow\downarrow}/g = 0.9$ for illustration. In Fig. 5(b), we show that, with increasing of β , the system first undergoes a transition from the SP-II to HSL phase at a critical point β_{c1} . Then, the system enters into the PW phase near the critical line. Finally, as the intralayer coupling approaches $\beta_{c3} \simeq 1$, the momenta of the energy minima shrink to $\mathbf{Q} = \mathbf{0}$ and all atoms condense in the zero-momentum phase (ZMP). All these quantum phases can be observed through the spin-resolved time-of-flight measurements of the density profiles, the momentum distributions, and spin textures.

Finally, we discuss a more general case with the asymmetric intra-species interaction $g_{\uparrow} \neq g_{\downarrow}$. Both the variation and numerical results show that, although the phase

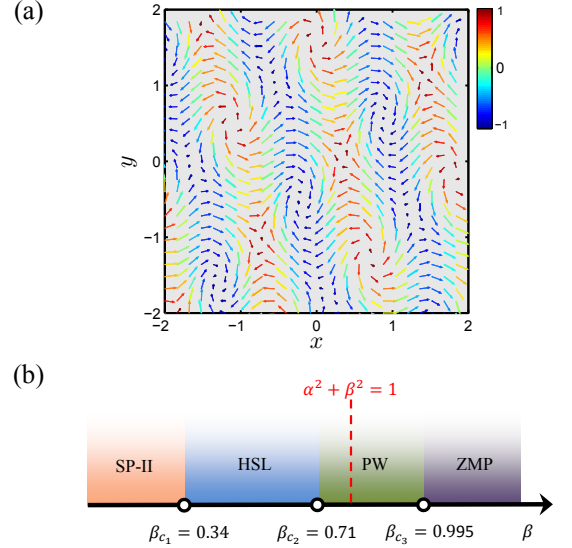


FIG. 5: (Color online) (a) Spin texture of the up layer for the HSL phase represented in Fig. 4. The color of the arrows indicates the magnitude of S_{iz} . (b) Phase transitions as a function of the intralayer coupling β , where the interlayer tunneling is fixed by $\alpha = 0.6$, and $g_{\uparrow\downarrow}/g = 0.9$.

boundaries get modified, the phase diagram as a function of α and $g_{\uparrow\downarrow}/\sqrt{g_{\uparrow}g_{\downarrow}}$ bears similar structure as Fig. 1, see the Sec.C of the Supplementary material [58] for more details. Thus all the predicted quantum phases survive and the TP still occurs on the critical line, demonstrating that these are unique and universal features of the bilayer system for a wide range of atomic interaction parameters.

In conclusion, we have investigated the ground state structures of a bilayer BEC subjected to a 1D intralayer SOC which is different for each layer. Due to an interplay between the interlayer tunneling, intralayer SOC and atomic interactions, the ground states display a rich phase diagram. It is demonstrated that a new type of stripe phase which breaks the TR symmetry and a half-skyrmion lattice emerge spontaneously in the ground states. Furthermore, we predict the occurrence of a characteristic tetracritical point, where the four different quantum phases merge together. Such diverse phases emerge without including a strong trapping potential, a distinctive feature of the bilayer system in which only the atoms situated in the same layer interact repulsively.

We acknowledge H. Zhai, X. F. Zhang, S.-C. Gou, and L. Santos for helpful discussions. This work is supported by NCET, NSFC under grants Nos. 11347197, 61227902, NKBRSC under grants Nos. 2011CB921502, 2012CB821305, and the Lithuanian Research Council Project MIP-082/2012.

* Electronic address: gediminas.juzeliunas@tfai.vu.lt

[†] Electronic address: andrewjee@sina.com

- [1] M. Z. Hasan and C. L. Kane, Rev. Mod. Phys. **82**, 3045 (2010).
- [2] X. L. Qi and S. C. Zhang, Rev. Mod. Phys. **83**, 1057 (2011).
- [3] S. Sachdev, *Quantum Phase Transitions* (Cambridge University Press, 2011).
- [4] M. Lewenstein, A. Sanpera, V. Ahufinger, B. Damski, A. Sen(De), and U. Sen, Adv. Phys. **56**, 243 (2007).
- [5] I. Bloch, J. Dalibard, and W. Zwerger, Rev. Mod. Phys. **80**, 885 (2008).
- [6] J. Dalibard, F. Gerbier, G. Juzeliūnas, and P. Öhberg, Rev. Mod. Phys. **83**, 1523 (2011).
- [7] M. Lewenstein, A. Sanpera and V. Ahufinge, *Ultracold Atoms in Optical Lattices: Simulating quantum many-body systems* (Oxford University Press, Oxford, 2012).
- [8] N. Goldman, G. Juzeliūnas, P. Öhberg, I. B. Spielman, arXiv:1308.6533 (2013).
- [9] Y.-J. Lin, K. Jiménez-García, and I. B. Spielman, Nature (London) **471**, 83 (2011).
- [10] J.-Y. Zhang, S.-C. Ji, Z. Chen, L. Zhang, Z.-D. Du, B. Yan, G.-S. Pan, B. Zhao, Y.-J. Deng, H. Zhai, S. Chen, and J.-W. Pan, Phys. Rev. Lett. **109**, 115301 (2012).
- [11] P. J. Wang, Z.-Q. Yu, Z. K. Fu, J. Miao, L. H. Huang, S. J. Chai, H. Zhai, and J. Zhang, Phys. Rev. Lett. **109**, 095301 (2012).
- [12] L. W. Cheuk, A. T. Sommer, Z. Hadzibabic, T. Yefsah, W. S. Bakr, and M. W. Zwierlein, Phys. Rev. Lett. **109**, 095302 (2012).
- [13] C. Qu, C. Hamner, M. Gong, C. W. Zhang, P. Engels, Phys. Rev. A **88**, 021604(R) (2013).
- [14] H. Zhai, Int. J. Mod. Phys. B **26**, 1230001 (2013).
- [15] V. Galitski and I. B. Spielman, Nature **494**, 49 (2013).
- [16] C. J. Wang, C. Gao, C.-M. Jian, and H. Zhai, Phys. Rev. Lett. **105**, 160403 (2010).
- [17] T.-L. Ho and S. Z. Zhang, Phys. Rev. Lett. **107**, 150403 (2011).
- [18] Z. F. Xu, R. Lü, and L. You, Phys. Rev. A **83**, 053602 (2011).
- [19] Y. P. Zhang, L. Mao, and C. W. Zhang, Phys. Rev. Lett. **108**, 035302 (2012).
- [20] Y. Li, L. P. Pitaevskii, and S. Stringari, Phys. Rev. Lett. **108**, 225301 (2012).
- [21] J. P. Vyasnakere, S. Zhang, and V. B. Shenoy, Phys. Rev. B **84**, 014512 (2011).
- [22] H. Hu, L. Jiang, X.-J. Liu, and H. Pu, Phys. Rev. Lett. **107**, 195304 (2011).
- [23] M. Gong, S. Tewari, and C. W. Zhang, Phys. Rev. Lett. **107**, 195303 (2011).
- [24] Z.-Q. Yu and H. Zhai, Phys. Rev. Lett. **107**, 195305 (2011).
- [25] M. Gong, G. Chen, S.-T. Jia, and C. W. Zhang, Phys. Rev. Lett. **109**, 105302 (2012).
- [26] S. Sinha, R. Nath, and L. Santos, Phys. Rev. Lett. **107**, 270401 (2011).
- [27] H. Hu, B. Ramachandhran, H. Pu, and X.-J. Liu, **108**, 010402 (2012).
- [28] R. M. Wilson, B. M. Anderson, and C. W. Clark, Phys. Rev. Lett. **111**, 185303 (2013).
- [29] T. Kawakami, T. Mizushima, M. Nitta, and K. Machida Phys. Rev. Lett. **109**, 015301 (2012).
- [30] S. Mühlbauer, B. Binz, F. Jonietz, C. Pfleiderer, A. Rosch, A. Neubauer, R. Georgii, and P. Böni, Science **323**, 915 (2009).
- [31] X. Z. Yu, Y. Onose, N. Kanazawa, J. H. Park, J. H. Han, Y. Matsui, N. Nagaosa, and Y. Tokura, Nature (London) **465**, 901 (2010).
- [32] A. Schmeller, J. P. Eisenstein, L. N. Pfeiffer, and K. W. West, Phys. Rev. Lett. **75**, 4290 (1995).
- [33] G. E. Volovik, *The Universe in a Helium Droplet* (Clarendon, Oxford, 2003).
- [34] T. D. Stanescu and V. Galitski, Phys. Rev. B **75**, 125307 (2007).
- [35] A. Jacob, P. Öhberg, G. Juzeliūnas, and L. Santos, Appl. Phys. B **89**, 439 (2007).
- [36] G. Juzeliūnas, J. Ruseckas, M. Lindberg, L. Santos, and P. Öhberg Phys. Rev. A **77**, 011802(R) (2008).
- [37] G. Juzeliūnas, J. Ruseckas, and J. Dalibard, Phys. Rev. A **81**, 053403 (2010).
- [38] D. L. Campbell, G. Juzeliūnas, and I. B. Spielman, Phys. Rev. A **84**, 025602 (2011).
- [39] Z. F. Xu and L. You, Phys. Rev. A **85**, 043605 (2012).
- [40] B. M. Anderson, G. Juzeliūnas, V. M. Galitski, and I. B. Spielman, Phys. Rev. Lett. **108**, 235301 (2012).
- [41] B. M. Anderson, I. B. Spielman, and G. Juzeliūnas, Phys. Rev. Lett. **111**, 125301 (2013).
- [42] Z.-F. Xu, L. You, and M. Ueda, Phys. Rev. A **87**, 063634 (2013).
- [43] J. P. Eisenstein and A. H. MacDonald, Nature **432**, 691 (2004).
- [44] D.-W. Wang, Phys. Rev. Lett. **98**, 060403 (2007).
- [45] A. Pikovski, M. Klawunn, G. V. Shlyapnikov, and L. Santos, Phys. Rev. Lett. **105**, 215302 (2010).
- [46] A. C. Potter, E. Berg, D.-W. Wang, B. I. Halperin, and E. Demler, Phys. Rev. Lett. **105**, 220406 (2010).
- [47] S.-W. Su, I.-K. Liu, Y.-C. Tsai, W. M. Liu, and S.-C. Gou, Phys. Rev. A **86**, 023601 (2012).
- [48] J. Ruostekoski and J. R. Anglin, Phys. Rev. Lett. **86**, 3934 (2001).
- [49] J.-Y. Choi, W. J. Kwon, and Y. I. Shin, Phys. Rev. Lett. **108**, 035301 (2012).
- [50] P. M. Chaikin and T. C. Lubensky, *Principles of Condensed Matter Physics* (Cambridge University Press, Cambridge, England, 2000).
- [51] M. E. Fisher and D. R. Nelson, Phys. Rev. Lett. **32**, 1350 (1974).
- [52] H. Rohrer and C. Gerber, Phys. Rev. Lett. **38**, 909 (1977).
- [53] F. Gerbier and J. Dalibard, New J. Phys. **12**, 033007 (2010).
- [54] M. Aidelsburger, M. Atala, S. Nascimbène, S. Trotzky, Y. A. Chen, and I. Bloch, Phys. Rev. Lett. **107**, 255301 (2011).
- [55] M. Aidelsburger, M. Atala, M. Lohse, J. T. Barreiro, B. Paredes, and I. Bloch, Phys. Rev. Lett. **111**, 185301 (2013).
- [56] H. Miyake, G. A. Siviloglou, C. J. Kennedy, W. C. Burton, and W. Ketterle, Phys. Rev. Lett. **111**, 185302 (2013).
- [57] M. Atala, M. Aidelsburger, M. Lohse, J. T. Barreiro, B. Paredes, and I. Bloch, arXiv:1402.0819 (2014).
- [58] Supplemental Material.
- [59] W. S. Cole, S. Z. Zhang, A. Paramekanti, and N. Trivedi, Phys. Rev. Lett. **109**, 085302 (2012).
- [60] K. Kasamatsu, M. Tsubota, and M. Ueda, Phys. Rev. A **71**, 043611 (2005).

SUPPLEMENTARY MATERIALS

A. Effective single-particle Hamiltonian of the bilayer BECs with intralayer 1D SOC

We consider a Bose gas of ultracold atoms characterized by two internal (quasi-spin) states labelled by the index $\sigma = \uparrow, \downarrow$. The atoms are subjected to a double-well like optical potential in the z direction, and their motion is not confined in the xy plane. The single-particle Hamiltonian is given by

$$\hat{\mathcal{H}}_0 = \hat{\mathcal{H}}_1 + \hat{\mathcal{H}}_2 + \hat{\mathcal{H}}_3, \quad (\text{S1})$$

where the first term $\hat{\mathcal{H}}_1$ corresponds to the unperturbed atomic motion, the other two terms being due to the laser induced transitions between the two atomic internal states, as well as the laser assisted tunnelling of atoms between the two wells. The former $\hat{\mathcal{H}}_1$ reads in the second quantized representation

$$\hat{\mathcal{H}}_1 = \int d^2\mathbf{r} dz \sum_{\sigma=\uparrow,\downarrow} \hat{\psi}_\sigma^\dagger(\mathbf{r}, z) \left[-\frac{\nabla_{\mathbf{r}}^2 + \nabla_z^2}{2m} + V_{\text{op}}^\sigma(z) \right] \hat{\psi}_\sigma(\mathbf{r}, z), \quad (\text{S2})$$

where $\hat{\psi}_\sigma(\mathbf{r}, z)$ is an operator for annihilation of an atom positioned at $\{\mathbf{r}, z\}$ and in an internal state σ . Here \mathbf{r} is a 2D radius vector describing the atomic motion within a layer in the xy plane, the coordinate z characterizes the interlayer motion, and $V_{\text{op}}^\sigma(z)$ is the state-dependent double-well optical potential along the z axis. Such a state-dependent optical potential can be implemented, for instance, using a spin-singlet ground state and a metastable spin-triplet excited state of alkaline-earth atoms [1].

Assuming that the atoms are tightly confined in individual wells forming the double well, one can expand the field operator entering Eq. (S2) as:

$$\hat{\psi}_\sigma(\mathbf{r}, z) = \sum_{j=1,2} \hat{\psi}_{j\sigma}(\mathbf{r}) \phi_{j\sigma}(z), \quad (\text{S3})$$

where $\hat{\psi}_{j\sigma}(\mathbf{r})$ is the operator for annihilation of an atom in the j -th layer and the internal state σ , and $\phi_{j\sigma}(z)$ is the corresponding eigen-function for the atomic motion along the z axis. The latter $\phi_{j\sigma}(z)$ is localized in the j th well of the double-well potential and is characterized by the lowest energy $\varepsilon_{j\sigma}$ of that well:

$$\left[-\frac{\nabla_z^2}{2m} + V_{\text{op}}^\sigma(z) \right] \phi_{j\sigma}(z) = \varepsilon_{j\sigma} \phi_{j\sigma}(z). \quad (\text{S4})$$

Integrating over z in Eq. (S2), the two-layer Hamiltonian takes the form

$$\hat{\mathcal{H}}_1 = \int d^2\mathbf{r} \sum_{j=1,2;\sigma=\uparrow,\downarrow} \hat{\psi}_{j\sigma}^\dagger(\mathbf{r}) \left[\frac{\mathbf{q}^2}{2m} + \varepsilon_{j\sigma} \right] \hat{\psi}_{j\sigma}(\mathbf{r}). \quad (\text{S5})$$

where $\mathbf{q} = -i\hbar\nabla_{\mathbf{r}}$ is the momentum operator for the atomic motion in the xy plane. We consider an asymmetric double-well potential for which the direct inter-layer tunneling is inhibited due to a sufficiently large energy offset Δ_σ ($\Delta_\sigma \equiv \varepsilon_{1\sigma} - \varepsilon_{2\sigma} > 0$).

Within an individual layer $j = 1, 2$ the laser beams induce transitions between the atomic internal states with a frequency ω_j and a coupling strength Ω_j :

$$\hat{\mathcal{H}}_2 = \int d^2\mathbf{r} \sum_{j=1,2} \left[\Omega_j e^{i(\mathbf{k}_j \cdot \mathbf{r} - \omega_j t)} + c.c. \right] \hat{\psi}_{j\uparrow}^\dagger(\mathbf{r}) \hat{\psi}_{j\downarrow}(\mathbf{r}) + \text{H.c.}, \quad (\text{S6})$$

where the transitions are accompanied by a recoil momentum $\mathbf{k}_{1,2}$ along \hat{x} and \hat{y} axis, respectively.

Additionally, there is a laser-assisted tunneling of atoms between the layers without changing their internal state σ [2–5]. The corresponding interlayer atom-laser interaction is characterized by a frequency ω_σ , a coupling strength J_σ and a recoil momentum \mathbf{k}_σ in the xy plane, all of them being generally dependent on the atomic internal state $\sigma = \uparrow, \downarrow$. Thus one has

$$\hat{\mathcal{H}}_3 = \int d^2\mathbf{r} \sum_{\sigma=\uparrow,\downarrow} \left(J_\sigma e^{i(\mathbf{k}_\sigma \cdot \mathbf{r} - \omega_\sigma t)} + c.c. \right) \hat{\psi}_{2\sigma}^\dagger(\mathbf{r}) \hat{\psi}_{1\sigma}(\mathbf{r}) + \text{H.c.}, \quad (\text{S7})$$

where the strength of the interlayer coupling $J_\sigma = \Omega_\sigma \int dz \phi_{2\sigma}^*(z) \phi_{1\sigma}(z) e^{ik_z z}$ depends both on the Rabi frequency Ω_σ of the atom-light coupling and also on the overlap of the wave-functions $\phi_{1\sigma}(z)$ and $\phi_{2\sigma}(z)$ of individual wells. It is noteworthy that the laser-induced interlayer tunnelling can take place only if there is a momentum transfer k_z in the tunnelling direction z [4]. In fact, the eigen-states corresponding to each layer $\phi_{1\sigma}(z)$ and $\phi_{2\sigma}(z)$ are orthogonal, so it is the factor $e^{ik_z z}$ which makes the overlap integral J_σ non-zero.

To eliminate the spatial and temporal dependence in the Hamiltonian, let us perform a unitary transformation

$$\hat{U} = e^{-i\hat{S}t}, \quad \text{with} \quad \hat{S} = \int d^2\mathbf{r} \sum_{j=1,2;\sigma=\uparrow,\downarrow} (\varepsilon_{j\sigma} t + m_\sigma \mathbf{k}_j \cdot \mathbf{r}) \hat{\psi}_{j\sigma}^\dagger(\mathbf{r}) \hat{\psi}_{j\sigma}(\mathbf{r}), \quad (\text{S8})$$

where $m_\uparrow = 1/2$ and $m_\downarrow = -1/2$. The Hamiltonian $\hat{\mathcal{H}}_0$ transforms to $\hat{H}_{\text{eff}} = \hat{U}^\dagger \hat{\mathcal{H}}_0 \hat{U} - i\hbar \hat{U}^\dagger \partial_t \hat{U}$, where the last term, due to the time-dependence of \hat{U} , eliminates the energies $\varepsilon_{j\sigma}$ featured in the Hamiltonian $\hat{\mathcal{H}}_1$, Eq. (S5). Additionally, the operators entering $\hat{\mathcal{H}}_2$ and $\hat{\mathcal{H}}_3$ acquire extra time- and position-dependent factors: $\hat{U}^\dagger \hat{\psi}_{j\uparrow}^\dagger(\mathbf{r}) \hat{\psi}_{j\downarrow}(\mathbf{r}) \hat{U} = \hat{\psi}_{j\uparrow}^\dagger(\mathbf{r}) \hat{\psi}_{j\downarrow}(\mathbf{r}) e^{i(\varepsilon_{j\downarrow} - \varepsilon_{j\uparrow} - \mathbf{k}_j \cdot \mathbf{r})t}$ and $\hat{U}^\dagger \hat{\psi}_{2\sigma}^\dagger(\mathbf{r}) \hat{\psi}_{1\sigma}(\mathbf{r}) \hat{U} = \hat{\psi}_{2\sigma}^\dagger(\mathbf{r}) \hat{\psi}_{1\sigma}(\mathbf{r}) e^{i[\varepsilon_{1\sigma} - \varepsilon_{2\sigma} + m_\sigma (\mathbf{k}_1 - \mathbf{k}_2) \cdot \mathbf{r}]t}$. We assume a resonant situation where $\omega_j = \varepsilon_{j\downarrow} - \varepsilon_{j\uparrow} \equiv \delta_j$ and $\omega_\sigma = \varepsilon_{1\sigma} - \varepsilon_{2\sigma} \equiv \Delta_\sigma$, and apply the rotating wave approximation by ignoring the fast temporal oscillating terms in the transformed Hamiltonian, corresponding to the *c.c.* terms in Eqs. (S6)-(S7). Consequently, one arrives at the time-independent single-particle Hamiltonian $\hat{H}_{\text{eff}} = \hat{\mathcal{H}}'_1 + \hat{\mathcal{H}}'_2 + \hat{\mathcal{H}}'_3$, with:

$$\hat{\mathcal{H}}'_1 = \int d^2\mathbf{r} \sum_{j=1,2;\sigma=\uparrow,\downarrow} \hat{\psi}_{j\sigma}^\dagger(\mathbf{r}) \frac{(\mathbf{q} + m_\sigma \mathbf{k}_j)^2}{2m} \hat{\psi}_{j\sigma}(\mathbf{r}). \quad (\text{S9})$$

$$\hat{\mathcal{H}}'_2 = \int d^2\mathbf{r} \sum_{j=1,2} \Omega_j \hat{\psi}_{j\uparrow}^\dagger(\mathbf{r}) \hat{\psi}_{j\downarrow}(\mathbf{r}) + \text{H.c.}, \quad (\text{S10})$$

and

$$\hat{\mathcal{H}}'_3 = \int d^2\mathbf{r} \sum_{\sigma=\uparrow,\downarrow} J_\sigma e^{i[\mathbf{k}_\sigma \cdot \mathbf{r} + m_\sigma (\mathbf{k}_1 - \mathbf{k}_2) \cdot \mathbf{r}]t} \hat{\psi}_{2\sigma}^\dagger(\mathbf{r}) \hat{\psi}_{1\sigma}(\mathbf{r}) + \text{H.c.}, \quad (\text{S11})$$

where only the third term $\hat{\mathcal{H}}'_3$ has the position-dependence. In what follows we set the wave-vectors associated with the interstate and interlayer transitions to be matched in the xy plane: $\mathbf{k}_\sigma = m_\sigma (\mathbf{k}_2 - \mathbf{k}_1)$, i.e. $\mathbf{k}_{\uparrow,\downarrow} = \pm(\mathbf{k}_2 - \mathbf{k}_1)/2$. In that case the exponent featured in Eq. (S11) disappears, making the term $\hat{\mathcal{H}}'_3$ and hence the whole transformed Hamiltonian \hat{H}_{eff} position-independent. Introducing the two-component row and column bosonic field operators, $\hat{\psi}_j^\dagger(\mathbf{r}) = [\hat{\psi}_{j\uparrow}^\dagger(\mathbf{r}), \hat{\psi}_{j\downarrow}^\dagger(\mathbf{r})]$ and $\hat{\psi}_j(\mathbf{r}) = [\hat{\psi}_{j\uparrow}(\mathbf{r}), \hat{\psi}_{j\downarrow}(\mathbf{r})]^T$, and omitting a constant term, the Hamiltonian \hat{H}_{eff} can be represented as

$$\begin{aligned} \hat{H}_{\text{eff}} &= \int d^2\mathbf{r} \sum_{j=1,2} \hat{\psi}_j^\dagger(\mathbf{r}) \left[\frac{\mathbf{q}^2 + \mathbf{q} \cdot \mathbf{k}_j \sigma_z}{2m} + \Omega_j \sigma_x \right] \hat{\psi}_j(\mathbf{r}) \\ &+ \int d^2\mathbf{r} \sum_{\sigma=\uparrow,\downarrow} \left(J_\sigma \hat{\psi}_{1\sigma}^\dagger(\mathbf{r}) \hat{\psi}_{2\sigma}(\mathbf{r}) + \text{H.c.} \right), \end{aligned} \quad (\text{S12})$$

where Ω_j is taken to be real.

Finally we assume that the coupling strengths are state- and site-independent ($J_\sigma = J$ and $\Omega_j = \Omega$) and the SOC in each layer is along \hat{x} and \hat{y} directions, $\mathbf{q} \cdot \mathbf{k}_j = q_j k_j = 2q_j \lambda_j$, with $q_1 = q_x$ and $q_2 = q_y$. Setting a unit mass, $m = 1$, and interchanging the spin operators, $\sigma_x \rightarrow \sigma_z$ and $\sigma_z \rightarrow \sigma_x$, and one arrives at the single-particle second-quantised Hamiltonian given by Eq. (1) in the main text.

B. Ground state manifold of the single-particle Hamiltonian

In this section, we derive the ground manifold of the single-particle Hamiltonian. First, the energy spectrum of the lowest branch can be derived as

$$E(\tilde{\mathbf{q}})/E_\lambda = \tilde{q}^2 - \sqrt{2\tilde{q}^2 + \alpha^2 + \beta^2 + 2\sqrt{(\tilde{q}_x + \tilde{q}_y)^2[(\tilde{q}_x - \tilde{q}_y)^2 + \alpha^2]} + \alpha^2 \beta^2}. \quad (\text{S13})$$

To determine the energy minima for the chiral states, one needs to find the points where $\partial E(\tilde{\mathbf{q}})/\partial \tilde{q}_x = 0$ and $\partial E(\tilde{\mathbf{q}})/\partial \tilde{q}_y = 0$. This yields

$$\begin{aligned} 2\tilde{q}_x \sqrt{2\tilde{q}^2 + \alpha^2 + \beta^2 + 2\sqrt{(\tilde{q}_x + \tilde{q}_y)^2[(\tilde{q}_x - \tilde{q}_y)^2 + \alpha^2] + \alpha^2\beta^2}} - 2\tilde{q}_x - \frac{2\tilde{q}_x(\tilde{q}_x^2 - \tilde{q}_y^2) + \alpha^2(\tilde{q}_x + \tilde{q}_y)}{\sqrt{(\tilde{q}_x + \tilde{q}_y)^2[(\tilde{q}_x - \tilde{q}_y)^2 + \alpha^2] + \alpha^2\beta^2}} &= 0 \\ 2\tilde{q}_y \sqrt{2\tilde{q}^2 + \alpha^2 + \beta^2 + 2\sqrt{(\tilde{q}_x + \tilde{q}_y)^2[(\tilde{q}_x - \tilde{q}_y)^2 + \alpha^2] + \alpha^2\beta^2}} - 2\tilde{q}_y - \frac{2\tilde{q}_y(\tilde{q}_y^2 - \tilde{q}_x^2) + \alpha^2(\tilde{q}_x + \tilde{q}_y)}{\sqrt{(\tilde{q}_x + \tilde{q}_y)^2[(\tilde{q}_x - \tilde{q}_y)^2 + \alpha^2] + \alpha^2\beta^2}} &= 0. \end{aligned} \quad (\text{S14})$$

For $\alpha^2 + \beta^2 < 1$, there are four minimum chiral states at $\pm \mathbf{Q}_1 = \pm(\tilde{q}_0^+, \tilde{q}_0^-)$ and $\pm \mathbf{Q}_2 = \pm(\tilde{q}_0^-, \tilde{q}_0^+)$ in the above two equations. Here, $\tilde{q}_0^\pm = \frac{1}{2}(\sqrt{Q_0^2 + \alpha^2/2} \pm \sqrt{Q_0^2 - \alpha^2/2})$ with $Q_0 = |\mathbf{Q}_{1,2}|$ satisfying a nonlinear equation

$$\sqrt{2Q_0^2 + \alpha^2 + \beta^2 + 2\sqrt{(Q_0^2 + \alpha^2/2)^2 + \alpha^2\beta^2}} - \frac{Q_0^2 + \alpha^2/2}{\sqrt{(Q_0^2 + \alpha^2/2)^2 + \alpha^2\beta^2}} = 1. \quad (\text{S15})$$

The corresponding multicomponent eigen function is given by for four degenerate energy minima at $\tilde{\mathbf{q}} = \pm \mathbf{Q}_1$ and $\tilde{\mathbf{q}} = \pm \mathbf{Q}_2$

$$\Psi_{\tilde{\mathbf{q}}} \equiv \Phi_{\tilde{\mathbf{q}}} e^{i\tilde{\mathbf{q}} \cdot \mathbf{r}} = f(\tilde{\mathbf{q}}) \begin{pmatrix} \alpha [\beta \xi - \beta^2 - \zeta - (\tilde{q}_x + \tilde{q}_y)^2] \\ \alpha [\beta (\tilde{q}_x - \tilde{q}_y) - \xi (\tilde{q}_x + \tilde{q}_y)] \\ (\beta - \xi)(\tilde{q}_x^2 - \tilde{q}_y^2 - \zeta) - \alpha^2 \beta \\ 2\tilde{q}_y (\zeta - \tilde{q}_x^2 + \tilde{q}_y^2) + \alpha^2 (\tilde{q}_x + \tilde{q}_y) \end{pmatrix} e^{i\tilde{\mathbf{q}} \cdot \mathbf{r}}, \quad (\text{S16})$$

where $f(\tilde{\mathbf{q}})$ is the normalized coefficient, $\xi = \sqrt{\alpha^2 + \beta^2 + 2\tilde{q}^2 + 2\zeta}$, and $\zeta = \sqrt{\alpha^2\beta^2 + \alpha^2(\tilde{q}_x + \tilde{q}_y)^2 + (\tilde{q}_x^2 - \tilde{q}_y^2)^2}$.

When α is increased above the critical line with $\alpha^2 + \beta^2 = 1$, the minimum chiral states converge to $\pm \mathbf{Q}$ with $\mathbf{Q} = \sqrt{1 - \beta^2}(1/2, 1/2)$ on the diagonal axis. In this case, for strong intralayer coupling $\beta \geq 1$, the minima would shrink to $\mathbf{Q} = \mathbf{0}$.

C. Phase diagram for the asymmetric intra-species interaction

In the main text we have studied the symmetric situation where $g_\uparrow = g_\downarrow$. Now we discuss the asymmetric intra-species interaction $g_\uparrow \neq g_\downarrow$. One may wonder whether the predicted new quantum phases and the TP predicted are preserved in the asymmetric case. For this purpose we take $g_\uparrow/g_\downarrow = 0.95$ as an example, and calculate the phase diagram shown in Fig. S1. We find that although the phase boundaries get modified, the phase diagram as a function of α and $g_{\uparrow\downarrow}/\sqrt{g_\uparrow g_\downarrow}$ bears similar structure as that of the symmetric situation, demonstrating that these are the unique and universal features of the bilayer system. Note that the TP still appears on the critical line, but gets shifted by the asymmetric intra-species interaction.

* Electronic address: gediminas.juzeliunas@tfai.vu.lt

† Electronic address: andrewjee@sina.com

[1] F. Gerbier and J. Dalibard, New J. Phys. **12**, 033007 (2010).

[2] M. Aidelsburger, M. Atala, S. Nascimbene, S. Trotzky Y.-A. Chen, and I. Bloch, Phys. Rev. Lett. **107**, 255301 (2011).

[3] M. Aidelsburger, M. Atala, M. Lohse, J. T. Barreiro, B. Paredes, and I. Bloch, Phys. Rev. Lett. **111**, 185301 (2013).

[4] H. Miyake, G. A. Siviloglou, C. J. Kennedy, W. C. Burton, and W. Ketterle, Phys. Rev. Lett. **111**, 185302 (2013).

[5] M. Atala, M. Aidelsburger, M. Lohse, J. T. Barreiro, B. Paredes, and I. Bloch, arXiv:1402.0819 (2014).

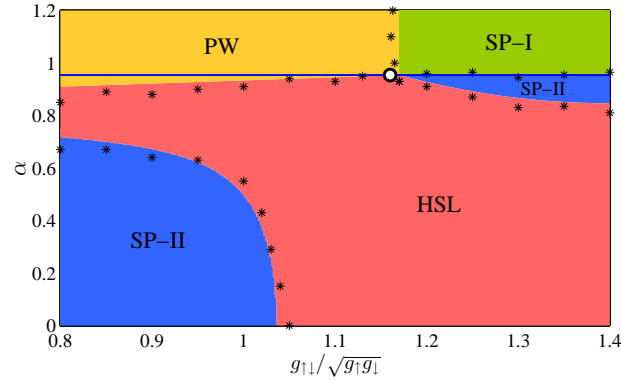


FIG. S1: (color online) Phase diagram of a bilayer BEC with a 1D interlayer SOC differently oriented for each layer as a function of the dimensionless interlayer tunneling α and $g_{\uparrow\downarrow}/\sqrt{g_{\uparrow}g_{\downarrow}}$ for the asymmetric intra-species interaction $g_{\uparrow}/g_{\downarrow} = 0.95$. The dimensionless intralayer coupling is set to be $\beta = 0.3$. The stars represent the phase boundaries determined from the numerical simulations and the colored regions are determined by the variational results. The horizontal solid line marks the critical line $\alpha^2 + \beta^2 = 1$.